J Mol Model (2013) 19:2375–2382
DOI 10.1007/s00894-013-1787-y

ORIGINAL PAPER

A comparative study on carbon, boron-nitride, boron-phosphide and silicon-carbide nanotubes based on surface electrostatic potentials and average local ionization energies

Mehdi D. Esrafili · Hadi Behzadi

Received: 14 November 2012 / Accepted: 28 January 2013 / Published online: 14 February 2013

Abstract A density functional theory study was carried out to predict the electrostatic potentials as well as average local ionization energies on both the outer and the inner surfaces of carbon, boron-nitride (BN), boron-phosphide (BP) and silicon-carbide (SiC) single-walled nanotubes. For each nanotube, the effect of tube radius on the surface potentials and calculated average local ionization energies was investigated. It is found that SiC and BN nanotubes have much stronger and more variable surface potentials than do carbon and BP nanotubes. For the SiC, BN and BP nanotubes, there are characteristic patterns of positive and negative sites on the outer lateral surfaces. On the other hand, a general feature of all of the systems studied is that stronger potentials are associated with regions of higher curvature. According to the evaluated surface electrostatic potentials, it is concluded that, for the narrowest tubes, the water solubility of BN tubes is slightly greater than that of SiC followed by carbon and BP nanotubes.

Keywords Carbon nanotube · Boron-nitride nanotube · Electrostatic potential · DFT · Average local ionization energies

Introduction

The discovery of carbon nanotubes (CNTs) by Iijima [1] has set off a tremendous explosion of general interest in these quasi-one-dimensional structures. Subsequent investigations have introduced stable tubular structures other than CNTs where the counterparts of atoms in the third and fifth groups of elements (III–V) have been proposed as proper materials [2–8]. To date, the properties of boron-nitride nanotubes (BNNTs) [9, 10] and boron-phosphide nanotubes (BPNTs) [11–13] have been investigated by numerous experimental and computational methods. It is well-documented that, due to their small covalent radius, carbon, boron and nitrogen atoms can generate considerable strain energy, preventing the formation of the close-packed structures with larger coordination found in clusters of covalent elements with larger radii such as silicon [14]. Consequently, carbon and boron-nitride can form very stable low-dimensional structures with smaller coordination. By contrast, low coordinated structures of Si, graphitic or cage-like, are predicted to be unstable [15, 16]. The possibility exists, however, that substitutional doping of tubular Si structures by a sufficient number of C atoms may render it stable. This is because both C–C and Si–C bonds are known to be stronger than the Si–Si bonds and can counteract the instability in nanotubes containing only Si–Si bonds.

As for electrical conductivity, unlike CNTs, BNNTs, BPNTs and SiCNTs are viewed as always being semiconductors, with almost constant band gap that is nearly independent of tubular diameter and chirality [17–20]. BNNTs and SiCNTs have many advantages over CNTs because their exterior surfaces have high reactivity, facilitating sidewall decoration and stability at high temperature [21, 22]. Due to the different electronegativities of their atomic counterparts, BNNTs and SiCNTs make intrinsically excellent sensors for the detection of some harmful gases, such as CO, HCN [19], NO, N_2O [22], NO_2 [23], CO_2 [24] and O_2 [25]. On the other hand, the longer bond length of Si–C (1.80 Å) compared to those of B–N (1.44 Å) and C–C (1.42 Å) makes SiCNTs more appropriate candidates for applications in

M. D. Esrafili (✉)
Laboratory of Theoretical Chemistry, Department of Chemistry, University of Maragheh, PO Box: 5513864596, Maragheh, Iran
e-mail: esrafili@maragheh.ac.ir

H. Behzadi
Department of Chemistry, Kharazmi University, Mofatteh Avenue, Tehran, Iran

materials storage than BNNTs and CNTs [26]. Theoretical simulations for a series of transition metal atoms chemically adsorbed on the outer surface of SiCNTs have shown that they exhibit many interesting physical properties, such as metallic and magnetic properties [27]. In addition, electronic properties of SiCNTs can be manipulated by adsorption of SiH_3 and CH_3 radicals, which can form acceptor or donor levels, depending on their adsorption sites [28]. More recently, Wang and Liew [29] indicated that the adsorption of F on Si sites is more favorable than that on C sites due to the large electronegativity of F for both zigzag SiCNT (8,0) and armchair SiCNT (6,6). Their results also showed that attachment of the F atom on the walls of SiCNTs gives rise to significant changes in electronic and magnetic properties of SiCNTs.

Exploring the noncovalent interactions between molecules and nanostructures surfaces is rather critical in understanding reaction mechanisms and many important technological processes. Such interactions, e.g., physical adsorption, are attributed mainly to electrostatic effects [30, 31]. In order to characterize and provide some valuable information of the origin of physisorption processes, it is essential to characterize in detail the electrostatic potentials, $V(\mathbf{r})$, on their surfaces. Recently, Politzer and co-workers [32–34] analyzed theoretically the $V(\mathbf{r})$ on the surfaces of a group of CNTs, BNNTs and $C_{2x}B_xN_x$. In the current study, we extend the analysis to include additional types of nanotubes including BPNTs and SiCNTs. In addition, the properties of these systems are discussed based on average local ionization energies $\bar{I}(\mathbf{r})$ [35], the lowest values of reveal the locations of the least tightly held electrons, and thus the favored sites for reaction with electrophiles or radicals. Our major question is to understand the influence of tube diameter on the surface electrostatic potentials and average local ionization energy of different zigzag CNTs, BNNTs, BPNTs and SiCNTs. Moreover, the relative aqueous solvation tendencies of these systems are also discussed.

Theory

A molecule's electrostatic potential $V(\mathbf{r})$ and average local ionization energy $\bar{I}(\mathbf{r})$ have proven to be effective guides to its reactive behavior [36]. $V(\mathbf{r})$ is the potential that is created at any point $\mathbf{r}$ by the molecule's nuclei and electrons, and is given rigorously by

$$V(\mathbf{r}) = \sum_A \frac{Z_A}{|R_A - \mathbf{r}|} - \int \frac{\rho(\mathbf{r}')d\mathbf{r}'}{|\mathbf{r}' - \mathbf{r}|} \quad (1)$$

in which Z_A is the charge on nucleus A, located at R_A, and $\rho(\mathbf{r})$ is the molecule's electronic density. $V(\mathbf{r})$ is a physical quantity and can be obtained experimentally, or computationally. $V(\mathbf{r})$ will be positive or negative in a given region depending upon whether the contribution of the nucleus or that of the electrons is dominant there. In contrast to $V(\mathbf{r})$, $\bar{I}(\mathbf{r})$ is a defined property [35]:

$$\bar{I}(\mathbf{r}) = \frac{\sum_i \rho_i(\mathbf{r})|\varepsilon_i|}{\rho(\mathbf{r})} \quad (2)$$

In Eq. 2, $\rho_i(\mathbf{r})$ is the electronic density of the *i*th occupied atomic or molecular orbital and ε_i is its energy. $\bar{I}(\mathbf{r})$ is interpreted as the average energy needed to remove an electron at the point $\mathbf{r}$, the focus being upon the point in space rather than upon a particular orbital.

For studying interactive tendencies, $V(\mathbf{r})$ and $\bar{I}(\mathbf{r})$ are computed on the surface of the molecule and the results are labeled $V_S(\mathbf{r})$ and $\bar{I}_S(\mathbf{r})$, respectively. These have been found to be complementary [37]. $V_S(\mathbf{r})$ is effective for noncovalent interactions, which are largely electrostatic in nature [38, 39], while $\bar{I}_S(\mathbf{r})$ is more suitable for charge transfer, bond formation, etc. [35].

Computational aspects

All density functional theory (DFT) calculations were performed using the GAMESS electronic structure package [40]. The geometries for all stationary points were optimized using the B3LYP/6-31G* level of theory. This level of theory is a reliable method that is commonly used in the study of different nanostructures [41].

Electrostatic surface potentials and average local ionization energies values were calculated using the WFA program [42]. In order to characterize the electrostatic potential quantitatively over the entire molecular surface, we used several statistically defined global quantities, including the following [43]:

(1) The positive, negative and overall average potentials on the surface:

$$\overline{V}_S^+ = \frac{1}{m}\sum_{i=1}^{m} V_S^+(\mathbf{r}_i) \quad , \quad \overline{V}_S^- = \frac{1}{n}\sum_{i=1}^{n} V_S^-(\mathbf{r}_i) \ ,$$
$$\overline{V}s = \frac{1}{m+n}\left(\sum_{i=1}^{m} V_S^+(\mathbf{r}_i) + \sum_{i=1}^{n} V_S^-(\mathbf{r}_i)\right) \quad (3)$$

(2) The average deviation of $V_S(\mathbf{r})$:

$$\Pi = \frac{1}{m+n}\sum_{i=1}^{m+n} \left|V_S(\mathbf{r}_i) - \overline{V_S}\right| \quad (4)$$

As noted previously [43], Π is an index of the internal charge separation that is present even in molecules that have zero dipole moments due to symmetry, such as carbon dioxide or para-dinitrobenzene [44].

(3) The total variance of $V_S(\mathbf{r})$, σ^2_{total}:

$$\sigma^2_{total} = \sigma^2_+ + \sigma^2_- = \frac{1}{\alpha}\sum_{j=1}^{\alpha}\left[V_S^+(\mathbf{r}_j) - \overline{V_S}^+\right]^2 + \frac{1}{\beta}\sum_{k=1}^{\alpha}\left[V_S^-(\mathbf{r}_k) - \overline{V_S}^-\right]^2 \quad (5)$$

Results and discussion

Figure 1 shows side views of the optimized (*n*,0) CNTs, BNNTs, BPNTs and SiCNTs (*n*=5–7). We noted that the possible orientations of the bonds relative to the tube axis result in two nonequivalent types of bonds in the zigzag nanotubes; namely zigzag or axial. Our results show that, for all systems studied, the evaluated bond lengths depend slightly on the diameter of the tube (Fig. 1). On the other hand, the data obtained for the optimized BPNTs reveal that the axial bonds distances decrease with increase in the tube diameter, while the reverse trend is evident for the others.

For each nanotube studied, Table 1 summarizes the evaluated $V_S(\mathbf{r})$ quantities as well as the $\bar{I}_S(\mathbf{r})$ values discussed in the section on Theory above. To provide perspective, Table 1 gives these quantities for a group of model compounds (C_6H_6, $B_3N_3H_6$, $B_3P_3H_6$ and $Si_3C_3H_6$). Figures 2, 3, 4, and 5 show the computed $V(\mathbf{r})$ and $\bar{I}(\mathbf{r})$ on the outer surfaces of (6,0) nanotubes. For the each property, three different views are considered including a side view (middle) and top-views (left and right). In the following section, we will focus on the local reactivity descriptors to predict the reactivity of different atomic sites on the external surface of the CNTs, BNNTs, BPNTs and SiCNTs, separately.

Carbon nanotubes

Figure 2 displays the evaluated $V_S(\mathbf{r})$ and $\bar{I}_S(\mathbf{r})$ on the 0.001 a.u. surface of (7,0) single-walled $C_{48}H_{12}$ nanotube. The figure shows the locations of the various most positive and most negative $V_S(\mathbf{r})$, designated $V_{S,max}$ and $V_{S,min}$, and the highest and lowest $\bar{I}_S(\mathbf{r})$, $\bar{I}_{S,max}$ and $\bar{I}_{S,min}$. From Fig. 1, it is evident that, for the $C_{48}H_{12}$ tube, the electron-donating hydrogens cause the outer carbon surfaces to become negative, but only very weakly, with minima $V_{S,min}$ between −8.0 and −8.2 kcal mol^{-1}. These are located on the outside near the ends. The outer surfaces are entirely negative except for the ends, where the hydrogens are located. These negative outer surfaces are due to the electronic charge withdrawn from the hydrogens, which in turn are the most positive portions of these nanotubes, with $V_{S,max}$ approaching 25.4 kcal mol^{-1}, about 13 kcal mol^{-1} more than for the hydrogens in benzene (Table 1). The potentials on the inner surfaces reflect two

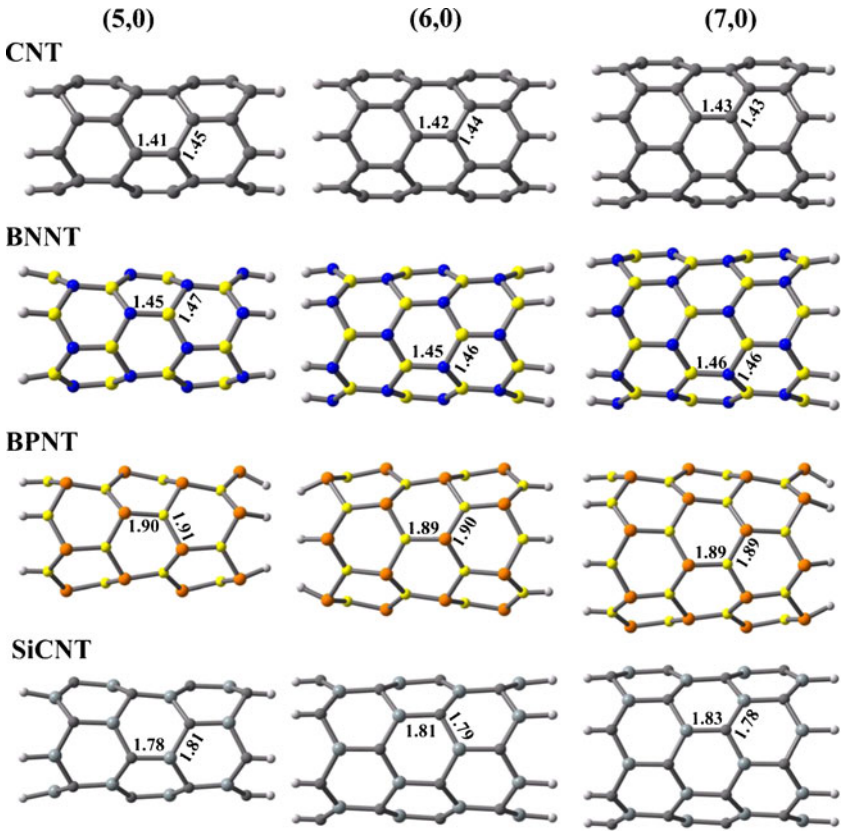

Fig. 1 Optimized structures and bond distances (in Å) of different (n,0) carbon nanotubes (CNTs), boron-nitride nanotubes (BNNTs), boron-phosphide nanotubes (BPNTs) and silicon-carbon nanotubes (SiCNTs)

Table 1 Calculated surface electrostatic potentials and average local ionization energy of different (*n*,0) nanotubes and model compounds

Tube	Diameter (Å)	A_S^+ (Å^2)[a]	A_S^- (Å^2)[a]	$\overline{V}_S^+$ (kcal mol^{-1})	$\overline{V}_S^-$ (kcal mol^{-1})	σ^2_{total}	Π (kcal mol^{-1})	$V_{S,max}$ (kcal mol^{-1})	$V_{S,min}$ (kcal mol^{-1})	$\bar{I}_{S,max}$ (eV)	$\bar{I}_{S,min}$ (eV)
(5,0)											
$C_{40}H_{10}$	3.71	124	209	15	−8	150	10.6	27.9	−13.2	13.8	7.6
$B_{20}N_{20}H_{10}$	3.90	135	208	17	−7	255	11.9	51.7	−20.1	14.1	8.6
$B_{20}P_{20}H_{10}$	5.13	370	162	8	−4	57	6.0	24.4	−9.9	12.4	7.8
$Si_{20}C_{20}H_{10}$	4.74	285	187	10	−9	119	9.2	25.9	−28.2	12.6	6.3
(6,0)											
$C_{48}H_{12}$	4.84	157	237	13	−7	188	9.0	25.4	−12.1	13.6	7.9
$B_{24}N_{24}H_{12}$	5.01	172	238	19	−8	280	13.0	51.5	−18.1	14.2	8.7
$B_{24}P_{24}H_{12}$	6.66	475	180	8	−4	52	5.8	22.5	−10.0	12.4	7.8
$Si_{24}C_{24}H_{12}$	6.14	319	266	16	−11	263	13.6	37.0	−30.9	12.1	6.1
(7,0)											
$C_{56}H_{14}$	5.23	173	300	11	−5	81	7.6	20.3	−8.2	13.3	8.2
$B_{28}N_{28}H_{14}$	5.48	217	270	19	−8	277	13.3	50.9	−16.8	14.2	8.7
$B_{28}P_{28}H_{14}$	7.24	570	197	7	−3	45	5.2	22.4	−10.2	12.4	7.8
$Si_{28}C_{28}H_{14}$	6.75	355	341	25	−17	597	21.5	53.3	−43.7	12.5	5.4
models											
C_6H_6	–	71	54	7	−9	80	7.8	12.0	−17.5	13.7	9.0
$B_3N_3H_6$	–	43	85	13	−5	112	8.2	31.7	−11.3	13.8	9.1
$B_3P_3H_6$	–	87	82	7	−5	54	6.0	16.1	−10.9	12.5	7.5
$Si_3C_3H_6$	–	115	49	5	−7	40	5.0	14.5	−14.0	12.2	7.4

[a] A_S^+ and A_S^- refer to positive and negative surface area, respectively

opposing factors: the negative charge gained from the hydrogens versus the closer proximity to more positive carbon nuclei. In the narrowest of these tubes—(5,0) $C_{40}H_{10}$—the latter effect seems to dominate and its inner surface is virtually completely positive. As the tube radius increases from (5,0) to (7,0), however, the proximity factor becomes less significant and more of the inner surface becomes negative. The greater variation in the surface potentials of the (5,0) and (6,0) CNTs can be seen in the magnitudes of Π and σ^2_{total}, which are distinctly larger than for the corresponding fullerene-like systems [32, 33]. However, due to the above mentioned opposing factors, there is no regular trend for the magnitudes of Π and σ^2_{total} from the (5,0) tube to the (7,0) tube. We noted that for the (7,0) CNT, the dominant theme, especially in side walls, is

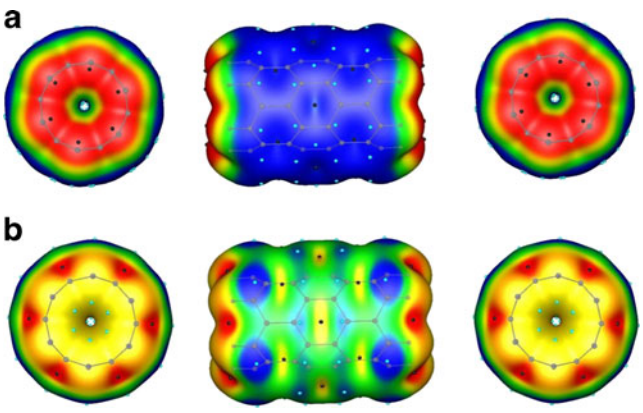

Fig. 2 Computed surface electrostatic potential (**a**) and average ionization potential energy (**b**) of the (6,0) $C_{48}H_{12}$ nanotube. Color ranges for $V_S(\mathbf{r})$, in kcal mol^{-1}: *red* >17.72, *yellow* 8.19–17.72, *green* −1.35–8.19, and *blue* <−1.35. Color ranges for $\bar{I}(\mathbf{r})$, in eV: *red* >12.58, *yellow* 11.28–12.58, *green* 9.99–11.28, *blue* <9.99. *Black circles* Surface maxima, *blue* surface minima

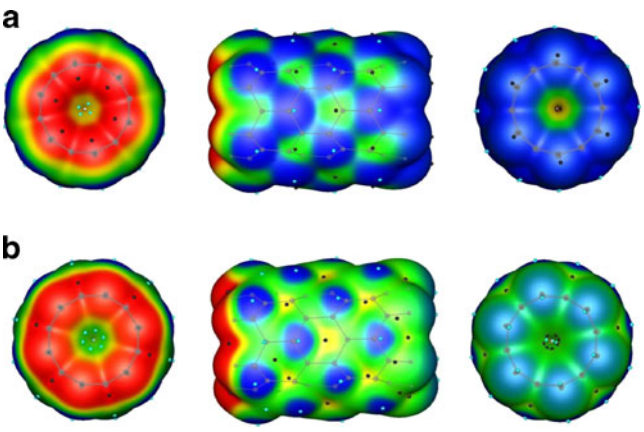

Fig. 3 Computed surface electrostatic potential (**a**) and average ionization potential energy (**b**) of the (6,0) $B_{24}N_{24}H_{12}$ nanotube. Color ranges for $V_S(\mathbf{r})$, in kcal mol^{-1}: *red* >39.78, *yellow* 19.33–39.78, *green* −1.12–19.33, *blue* <−1.12. Color ranges for $\bar{I}(\mathbf{r})$, in eV: *red* >13.23, *yellow* 11.76–13.23, *green* 10.29–11.76, *blue* <10.29. *Black circles* Surface maxima, *blue* surface minima

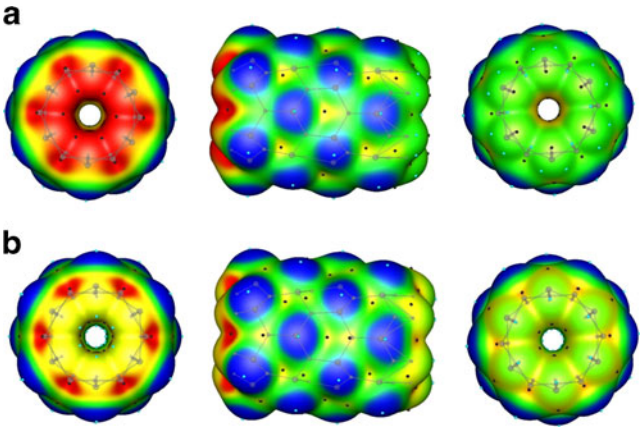

Fig. 4 Computed surface electrostatic potential (**a**) and average ionization potential energy (**b**) of the (6,0) $B_{24}P_{24}H_{12}$ nanotube. Color ranges for $V_S(\mathbf{r})$, in kcal mol^{-1}: *red* >16.78, *yellow* 7.28–16.78, *green* −2.22–7.28, *blue* <−2.22. Color ranges for $\bar{I}(\mathbf{r})$, in eV: *red* >12.33, *yellow* 11.01–12.33, *green* 9.69–11.01, *blue* <9.69. *Black circles* Surface maxima, *blue* surface minima

near-zero weakness and softness, showing relatively little variation (σ^2_{total}=188 kcal mol^{-1}) and small Π value.

According to Fig. 1b, the lowest $\bar{I}_{S,min}$ values of (6,0) $C_{48}H_{12}$ are associated with the capped carbons, and are fully consistent with the known tendency of electrophiles/radicals to react with the these sites. Thus, there is an $\bar{I}_{S,min}$ above each carbon atom as benzene, but not at the midpoint of the C–C bonds in ethylene, in which the π electrons are localized. Moreover, the magnitudes of $\bar{I}_{S,min}$ tend to be lower for carbon nanotubes than for benzene or graphene [34], indicating that the curvatures of the tubes increase their reactivity. A particularly noteworthy finding is also that the highest $\bar{I}_{S,max}$ are associated with the center of rings, with $\bar{I}_{S,max}$ values between 11.2 and 12.1 eV. These calculated $\bar{I}_{S,max}$ values are slightly greater than those of benzene (Table 1).

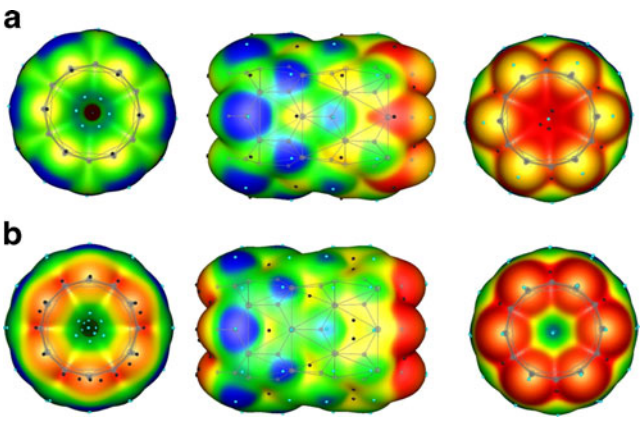

Fig. 5 Computed surface electrostatic potential (**a**) and average ionization potential energy (**b**) of the (6,0) $Si_{24}C_{24}H_{12}$ nanotube. Color ranges for $V_S(\mathbf{r})$, in kcal mol^{-1}: *red* >22.91, *yellow* 3.83–22.91, *green* −15.25–3.82, *blue* <−15.25. Color ranges for $\bar{I}(\mathbf{r})$, in eV: *red* >11.35, *yellow* 9.63–11.35, *green* 7.91–9.63, *blue* <7.91. *Black circles* Surface maxima, *blue* surface minima

Moreover, one can see that there is a usual tendency to weaken $\bar{I}_{S,max}$ values as the radius of CNTs increases.

Boron-nitride nanotubes

From Fig. 3a, it can be seen that BNNT surfaces are quite interesting. They all have regular patterns of positive and negative potentials associated with the boron and nitrogen atoms, respectively. Unlike CNTs, in which the hydrogens are always positive, they can now be either positive or negative, depending upon whether attached to a nitrogen or a boron. Figure 3a indicates that for the (6,0) BNNT, the interiors are positive and the calculated $V_{S,max}$ values decrease as the diameter of the tube increases. As in the case of the CNT analogue, the small diameter (5,0) BNNT has notably stronger and more variable positive and negative regions (Table 1). This is again due to the high degree of curvature on the sides and at the caps. On the outer lateral surfaces of the BNNTs, the positive regions above the borons are stronger than the negative ones of the nitrogen. The most positive regions are associated with hydrogen atoms located at the N-tip: the $V_{S,max}$ is about 51 kcal mol^{-1}, greater than those of borazine, ca. 31.7 kcal mol^{-1}. The greater variation in the surface potential of these BNNTs can be seen in the magnitude of σ^2_{total}, which is now markedly larger than for the corresponding CNTs. Furthermore, these tubes clearly show local B^+H^- polarity at one end and N^-H^+ at the other (Fig. 3a). This is evident in values of Π, our measure of internal charge distribution (Table 1). In particular, the N^-H^+ polarity of (5,0) tube is notable, the hydrogen potentials being about 51.7 kcal mol^{-1} and the capped nitrogens, −20.1 kcal mol^{-1}.

More interesting are the average local ionization energies on the BNNTs surfaces. Of primary interest are the magnitudes and locations of the lowest values of $\bar{I}_S$, the local minima $\bar{I}_{S,min}$. These reveal the least tightly held, most reactive electrons, which should be the sites most vulnerable to electrophilic or to free radical attack. The lowest of these $\bar{I}_{S,min}$ are those of nitrogen atoms located at N-tip, as can be seen very clearly in Fig. 3b. Moreover, a particularly interesting finding is that the sites of the lowest $\bar{I}_{S,min}$ in the BNNT are associated with the highest occupied molecular orbital (HOMO). This emphasizes the complementary of the frontier molecular orbital approach and $\bar{I}_S(\mathbf{r})$ to predict the reactivity of BNNTs. The evaluated $\bar{I}_{S,max}$ in Fig. 3b are in the general neighborhood of 14.1 eV. For comparison, the calculated $\bar{I}_{S,max}$ values of borazine, which are located above boron atoms are 13.8 eV (see Table 1).

Boron-phosphide nanotubes

Table 1 and Fig. 4a show that the surface electrostatic potentials in BPNTs are slightly different and quite soft.

Essentially the entire surfaces, both inner and outer, are positive $\left(A_S^+ > A_S^-\right)$ but only weakly so: $\overline{V}_S^+ = 8\text{kcal/mol}$ and $\overline{V}_S^- = -4\text{kcal/mol}$. The surface potentials are dominated by the weak positive and negative regions associated with the terminal boron and phosphorous atoms, respectively. The $V_{S,max}$ and $V_{S,min}$ are on the outer surfaces, both are weaker than for the BNNTs. Table 1 indicates that the evaluated surface $V_{s,max}$ and $V_{s,min}$ values of the (5,0) BPNT are 24.4 and −9.9 kcal mol^{-1}, respectively. More especially, Fig. 3a indicates that hydrogen atoms attached to the P-tip are positive, while those attached to the B-tip are slightly negative. Thus, V_S (**r**) would predict electrophilic attack to occur preferentially at the boron sites. On the other hand, the variability of surface potential diminishes for BPNTs; Π and σ^2_{total} decrease considerably from BNNTs to the corresponding BPNTs (Table 1). We noted that the positive regions above the borons are weaker than BNNT, 6.9 to 14.3 kcal mol^{-1}, and the negative ones of the P atoms are slightly weak, −5.2 to −10.2 kcal mol^{-1}. The inner surface is still positive, but not as strongly so, reaching ~5 kcal mol^{-1}. These tubes clearly show a weaker local B^+H^- polarity at one end and P^-H^+ at the other (Fig. 3a). Therefore, the corresponding Π values are smaller than those of BNNTs.

Comparison with the boron $\bar{I}_{S,max}$ of BNNT correctly predicts that, in the BPNTs, the phosphorus atoms tend to deactivate the ring toward nucleophilic attack. The computed $\bar{I}_{S,min}$ associated with phosphorous atoms are slightly smaller than those of nitrogens in BNNTs, due to the lower atomization energy of P atoms compared to N. As in the case of the BNNT analogue, there is clearly a marked tube-long trend from higher $\bar{I}_S$(**r**) to lower values in moving from phosphorous to the boron cap.

Silicon-carbon nanotubes

Structurally, SiCNT is composed from alternative C and Si layers. Inspection the surface electrostatic potentials maps obtained for (5,0), (6,0) and (7,0) SiCNTs indicates that they all have corresponding negative and positive surfaces. Further, the calculated $V_{S,max}$ and $V_{S,min}$ values of the SiCNTs are larger in magnitude than others discussed above. Considering the (6,0) tube, it is found that the $V_{S,min}$ of SiCNT is 19 kcal mol^{-1} more negative than those of its CNT analogue (Table 1). This indicates that SiCNTs are much better candidates to interact with nucleophiles than CNTs, BNNTs and BPNTs. Similar to what was found for the BPNTs, the major portion of the total surfaces of SiCNTs is now positive: $A_S^+ > A_S^-$. Figure 5a indicates that, on the outer lateral surfaces of the SiCNT, the positive regions above the silicon atoms are stronger than the negative ones of the carbons. The former have local maxima of 8 to 53 kcal mol^{-1}, while the local minima of the latter are only −7 to −44 kcal mol^{-1}. We note that these potentials are stronger than the corresponding $V_{S,max}$ and $V_{S,min}$ values of the model $Si_3C_3H_6$ compound (Table 1). At the Si capped ends of the tube, however, where the curvature is greatest, the positive potentials do reach 53 kcal mol^{-1}. The inner surfaces of all SiCNTs are very negative (Fig. 4a), the potential ranging between −7 and −27 kcal mol^{-1}. The terminal hydrogens of SiCNTs provide some electronic charge to the capped carbon atoms and these become slightly negative. Table 1 also indicates that for a given (*n*,0) tube, the evaluated Π of SiCNTs are greatest of any of the systems in Table 1. This is not surprising, given their obviously highly polar structures.

Figure 5b shows explicitly that the lowest $\bar{I}_{S,min}$ are associated with the capped carbon atoms. In general, there is an $\bar{I}_{S;min}$ above each carbon, as in $Si_3C_3H_6$. These $\bar{I}_{S,min}$ range from 5.0 to 9.4 eV, i.e., slightly smaller than those of carbon atoms in CNTs. On the other hand, there is the usual tendency of $I_{S,min}$ to weaken as the radius of the tube increases: it decreases from 6.3 eV for the (5,0) SiCNT to 5.4 eV for the (7,0). Thus, the carbon atoms in the former models have greater atomization energies than the latter. Figure 5b also reveals that the evaluated local maxima of $\bar{I}_{S,max}$ are associated with the centers of rings, correctly indicating these sites to be most susceptible to nucleophiles. Moreover, since the $\bar{I}_{S,max}$ of SiCNTs are slightly less than those found for CNTs at this computational level, this demonstrates the well-known deactivation of the ring by Si-doping.

According to earlier studies [32, 33], the computed $V_{S,max}$ can be used to obtain some rough qualitative insight into the relative solubilities of model nanotubes. It was shown, however, that $V_{S,max}$ plays a prominent role in determining the free energy of solvation, ΔG_{solv}, in water; ΔG_{solv} becomes more negative as $V_{S,max}$ increases. In Fig. 6, we found a rather good correlation between the calculated dipole moments and $V_{S,max}$ values of BNNT, BPNTs and SiCNTs. Thus, from the data shown in Table 1, it is concluded that, for the narrowest tubes, the water solubility of BNNT is slightly larger than those of SiCNTs followed by CNTs and BPNTs. On the other hand, as

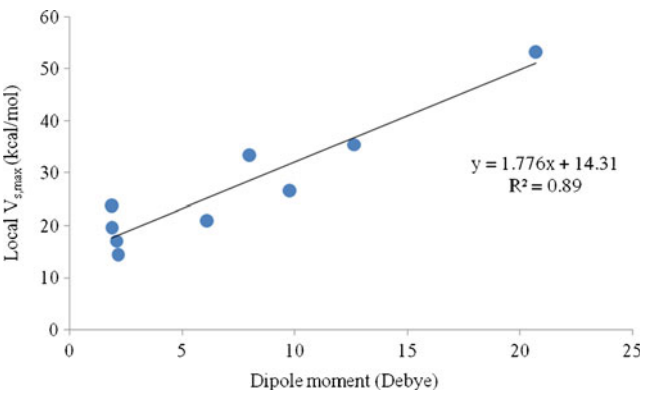

Fig. 6 Correlation between local $V_{S,max}$ values and dipole moments of different models of BNNTs, BPNTs and SiCNTs

the diameter of the CNTs, BNNTs and BPNTs increases, our calculations indicate that the solubility of the tubes decreases.

Conclusions

In this study, we characterized the surface electrostatic potentials as well as average local ionization energies of 12 carbon, BN, BP and SiC model nanotubes. Some results are:

(1) The strengths and variabilities of the inner and outer surface electrostatic potentials increase considerably in going from BPNT to CNT, BNNT and SiCNT.
(2) The lowest $\bar{I}_{S,min}$ values of the zigzag CNTs are associated with capped carbons, and are fully consistent with the known tendency of electrophiles/radicals to react with the these sites.
(3) The small diameter (5,0) BNNT has notably stronger and more variable positive and negative regions. This is again due to the high degree of curvature on the sides and at the caps.
(4) For BPNTs, the positive regions above the borons are weaker than BNNT, 6.9 to 14.3 kcal mol^{-1}, and the negative ones of the P atoms are slightly weak, −5.2 to −10.2 kcal mol^{-1}. These tubes clearly show a weaker local $B^{+}H^{-}$ polarity at one end and $P^{-}H^{+}$ at the other. Therefore, the corresponding Π values are smaller than those of BNNTs.
(5) Similar to what was found for the BPNTs, the major portion of the total surfaces of SiCNTs is positive: $A_S^+ > A_S^-$. On the outer lateral surfaces of each SiCNT, the positive regions above the silicon atoms are stronger than the negative ones of the carbons.
(6) Based on the evaluated surface electrostatic potentials, we found an acceptable correlation between the calculated dipole moments and $V_{S,max}$ values of BNNTs, BPNTs and SiCNTs.

References

1. Iijima S (1991) Helical microtubules of graphitic carbon. Nature 354:56–58
2. Malek K, Sahimi M (2010) Molecular dynamics simulations of adsorption and diffusion of gases in silicon-carbide nanotubes. J Chem Phys 132:014310
3. Teo BK (2003) Doing chemistry on low-dimensional silicon surfaces: silicon nanowires as platforms and templates. Coord Chem Rev 246:229–246
4. Ahmed R, Fazal-e-Aleem, Hashemifar SJ, Akbarzadeh H (2008) First-principles study of the structural and electronic properties of III-phosphides. Physica B 403:1876–1881
5. Guo CS, Fan WJ, Chen ZH, Zhang RQ (2006) First-principles study of single-walled armchair $C_x(BN)_y$ nanotubes. Solid State Commun 137:549–552
6. Beheshtian J, Behzadi H, Esrafili MD, Shirvani BB, Hadipour NL (2010) A computational study of water adsorption on boron nitride nanotube. Strut Chem 21:903–908
7. Hou S, Shen Z, Zhang J, Zhao X, Xue Z (2004) Ab initio calculations on the open end of single-walled BN nanotubes. Chem Phys Lett 393:179–183
8. Zhang D, Zhang RQ (2003) Ab initio calculations on the open end of single-walled BN nanotubes. Chem Phys Lett 371:426–432
9. Zhi C, Bando Y, Tang C, Golberg D (2010) Boron nitride nanotubes. Mater Sci Eng 70:92–111
10. Akdim B, Pachter R, Duan X, Adams WW (2003) Comparative theoretical study of single-wall carbon and boron-nitride nanotubes. Phys Rev B 67:245404
11. Schroten E, Goossens A, Schoonman J (1998) Photo- and electroreflectance of cubic boron phosphide. J Appl Phys 83:1660–1663
12. Ferreira VA, Leite Alves HW (2008) Boron phosphide as the buffer-layer for the epitaxial III-nitride growth: a theoretical study. J Cryst Growth 310:3973–3978
13. Mirzaei M (2011) Carbon doped boron phosphide nanotubes: a computational study. J Mol Model 17:89–96
14. Menon M, Richter E, Andriotis AN (2004) Structure and stability of SiC nanotubes. Phys Rev B 69:115322
15. Khan F, Broughton J (1991) Relaxation of icosahedral-cage silicon clusters via tight-binding molecular dynamics. Phys Rev B 43:11754
16. Menon M, Subbaswamy K (1994) Structure of Si60. Cage versus network structures. Chem Phys Lett 219:219–222
17. Wu A, Song Q, Yang L, Hao Q (2011) The stability and electronic structures of B or/and N doped SiC nanotubes: a first-principles study. Comput Theor Chem 977:92–96
18. Gali G, Kang HS (2008) Strain energy and electronic structures of silicon carbide nanotubes: density functional calculations. Phys Rev B 78:165425
19. Zhang SL (2001) Optimal helicity of single-walled carbon nanotube. Phys Lett A 285:207–211
20. Zhao MW, Xia YY, Li F, Zhang RQ, Lee ST (2005) Strain energy and electronic structures of silicon carbide nanotubes: density functional calculations. Phys Rev B 71:085312
21. Zhou Z, Zhao J, Chen Z, Gao X, Yan T, Wen B, Schleyer PR (2006) Comparative study of hydrogen adsorption on carbon and BN nanotubes. J Phys Chem B 110:13363–13369
22. Gao GH, Kang HS (2008) First principles study of NO and NNO chemisorption on silicon carbide nanotubes and other nanotubes. J Chem Theory Comput 4:1690–1697
23. Gao GH, Park SH, Kang HS (2009) A first principles study of NO_2 chemisorption on silicon carbide nanotubes. Chem Phys 355:50–54
24. Zhao JX, Ding YH (2009) Can silicon carbide nanotubes sense carbon dioxide? J Chem Theory Comput 5:1099–1105
25. Cao FL, Xu XY, Ren W, Zao CY (2010) Theoretical study of O_2 molecular adsorption and dissociation on silicon carbide nanotubes. J Phys Chem C 114:970–976
26. Mpourmpakis G, Froudakis GE, Lithoxoos GP, Samios J (2006) SiC nanotubes: a novel material for hydrogen storage. Nano Lett 6:1581–1583
27. Zhao JX, Ding YH (2008) Silicon carbide nanotubes functionalized by transition metal atoms: a density functional study. J Phys Chem C 112:2558–2564
28. Li F, Xia YY, Zhao MW, Liu XD, Huang BD, Yang ZH, Ji YJ, Song C (2005) Density-functional theory calculations of XH3-decorated SiC nanotubes (X = {C, Si}): structures, energetics, and electronic structures. J Appl Phys 97:104311
29. Wang X, Liew KM (2012) Density functional study of fluorinated single-walled silicon carbide nanotubes. J Phys Chem C 116:1702–1708
30. Naray-Szabo G, Ferenczy GG (1995) Molecular electrostatics. Chem Rev 95:829–847

31. Sauer J, Ugliengo P, Garrone E, Saunders VR (1994) Theoretical study of van der Waals complexes at surface sites in comparison with the experiment. Chem Rev 94:2095–2160
32. Peralta-Inga Z, Lane P, Murray JS, Boyd S, Grice ME, O'Connor CJ, Politzer P (2003) Characterization of surface electrostatic potentials of some (5,5) and (*n*,1) carbon and boron/nitrogen model nanotubes. Nano Lett 3:21–28
33. Politzer P, Lane P, Murray JS, Concha MC (2005) Comparative analysis of surface electrostatic potentials of carbon, boron/nitrogen and carbon/boron/nitrogen model nanotubes. J Mol Model 11:1–7
34. Politzer P, Murray JS, Lane P, Concha MC, Jin P, Peralta-Inga Z (2005) An unusual feature of end-substituted model carbon (6,0) nanotubes. J Mol Model 11:258–264
35. Politzer P, Murray JS, Bulat FA (2010) Average local ionization energy: a review. J Mol Model 16:1731–1742
36. Politzer P, Lane P, Concha MC, Ma Y, Murray JS (2007) An overview of halogen bonding. J Mol Model 13:305–311
37. Politzer P, Murray JS, Concha MC (2002) The complementary roles of molecular surface electrostatic potentials and average local ionization energies with respect to electrophilic processes. Int J Quantum Chem 88:19–27
38. Feynman RP (1939) Forces in molecules. Phys Rev 56:340–343
39. Hirschfelder JO, Curtiss CF, Bird RB (1954) Molecular theory of gases and liquids. Wiley, New York
40. Schmidt MW, Baldridge KK, Boatz JA, Elbert ST, Gordon MS, Jensen JH, Koseki S, Matsunaga N, Nguyen KA, Su SJ, Windus TL, Dupuis M, Montgomery JA (1993) General atomic and molecular electronic structure system. J Comput Chem 14:1347–1363
41. Esrafili MD, Behzadi H (2012) A DFT study on carbon-doping at different sites of (8, 0) boron nitride nanotube. Struct Chem. doi:10.1007/s11224-012-0110-3
42. Bulat FA, Toro-Labbe A, Brinck T, Murray JS, Politzer P (2010) Quantitative analysis of molecular surfaces: areas, volumes, electrostatic potentials and average local ionization energies. J Mol Model 16:1679–1691
43. Politzer P, Murray JS, Peralta-Inga Z (2010) Molecular surface electrostatic potentials in relation to noncovalent interactions in biological systems. Int J Quantum Chem 85:676–684
44. Brinck T, Murray JS, Politzer P (1992) Quantitative determination of the total local polarity (charge separation) in molecules. Mol Phys 76:609–617